Characterization and Electrical Properties of Individual Au–NiO–Au Heterojunction Nanowires

Jason S. Tresback, Alexander L. Vasiliev, Nitin P. Padture, Si-Young Park, and Paul R. Berger, *Senior Member, IEEE*

***Abstract*—High-definition metal–oxide–metal (MOM) heterojunction nanowires in the Au–NiO–Au system have been synthesized using a template-based method. These nanowires are ∼70 nm in diameter and ∼ 7 μm in total length, with a 100 to 300 nm wide NiO segment sandwiched between the Au nanowires axially. Detailed electron-microscopy characterization studies of these nanowires show that the oxide segment is primarily cubic NiO and nanocrystalline, and that both the Au–NiO interfaces are well-defined. These Au–NiO–Au nanowires have been incorporated into high-quality single-nanowire devices, fabricated using a direct-write method. The current–voltage (I–V) responses of individual Au–NiO–Au nanowires have been measured as a function of temperature in the range 298 to 573 K. While the I–V response at room temperature has been found to be nonlinear, it becomes more linear and less resistive with increasing temperature. These types of MOM nanowires are likely to offer certain advantages over all-oxide nanowires in fundamental size-effect studies, and they could be potentially useful as nanoscale building blocks for multifunctional nanoelectronics of the future.**

***Index Terms*—Electrical properties, electron microscopy, heterojunctions, nanowires, nickel oxide, single-nanowire devices, temperature effects.**

I. Introduction

OXIDE nanowires (nanoribbons, nanobelts, or nanorods) [1]–[6] are being used increasingly as 1-D building blocks in "bottom up" multifunctional nanoelectronics [7], taking advantage of the myriad size-dependent functional properties of oxides, such as electrical conductivity [5], ferroelectric [8], piezoelectric [9], electrooptic [3], magnetoresistance [10], [11], chemical-sensing [4], [5], [12], [13], and biosensing [14]. In this context, metal–oxide–metal (MOM) heterojunction nanowires, where a nanoscale segment of a functional oxide is sandwiched axially between two similar or dissimilar noble-metal nanowires, are likely to have some potential advantages over all-oxide nanowires (where the entire nanowire is an oxide), as discussed elsewhere [15]–[18]. Unlike all-oxide nanowires, where the electrical contacts between the oxide nanowire and device electrodes could be difficult to control and is limited by lithography, MOM nanowires provide metal–oxide contact integrated within the nanowire building block itself. The dimensions of the metallic segments can be varied easily in order to accommodate device fabrication methodologies, while the active oxide segment can be varied to modify electrical properties of the device. Furthermore, the MOM–nanowire architecture presents a rare opportunity to directly measure functional properties of nanoscale-volume oxides with well-defined dimensions and the absence of substrate affects.

NiO, an antiferromagnetic [19] wide-band-gap semiconductor (E_g ∼ 3.8 eV [20]) oxide, is used in magnetics [21], batteries [22], chemical sensing [23]–[26], mass flow/temperature sensing [27], electroluminescent [28], catalysis [29], fuel cells [30], and smart windows [31] applications. Recently, all-oxide 1-D NiO nanowires have been synthesized for use in some of these applications [32]–[36]. In contrast, recently Tresback *et al.* [15] reported a generic method for synthesizing Au–NiO–Au MOM nanowires. That method entails electroplating segmented metallic nanowires (e.g. Au–Ni–Au) inside nanoholes of anodic aluminum oxide (AAO) templates, followed by release and selective oxidation, resulting in isolated MOM nanowires (e.g. Au–NiO–Au). Here we have used this method to synthesize high-quality Au–NiO–Au nanowires of much smaller diameters of ∼70 nm. This method results in well-controlled, high-quality MOM nanowires, compared to methods described by others [18], and it affords easy dimensional tuning of the oxide segment. The resulting Au–NiO–Au nanowires have been characterized in some detail using transmission electron microscopy (TEM). Individual Au–NiO–Au nanowires were incorporated into devices using a direct-write method. In an effort to characterize the electrical properties of these MOM nanowires, their current–voltage (I–V) responses were measured as a function of temperature. These Au–NiO–Au MOM nanowires could be integrated as chemical nanosensors into "bottom up" multifunctional nanoelectronic devices of the future.

II. Experimental Procedure

A. Synthesis

The Au–NiO–Au MOM nanowires were synthesized using the procedure described by Tresback *et al.* [15]. Briefly, anodic aluminum oxide (AAO) templates with nanoholes diameter of ∼70 nm were prepared in-house. One side of the AAO templates was sealed by thermally evaporating a 0.5-μm Ag thin film, which served as the cathode for subsequent constant-current (0.5 mA) electroplating inside the nanoholes of the AAO templates. First, a small segment of Ag ($\sim$ 0.5 μm) was electroplated using 1025 Ag solution (Technic Inc., Cranston, RI). Next, one Au nanowire segment ($\sim$ 3 μm) was electroplated using an Orotemp-24 solution (Technic Inc., Cranston, RI) to

Manuscript received March 10, 2007; revised August 25, 2007. This work was supported by the National Science Foundation under Grant CTS 0514012.

J. S. Tresback, A. L. Vasiliev, and N. P. Padture are with the Department of Materials Science and Engineering, The Ohio State University Columbus, OH 43210, USA (e-mail: padture.1@osu.edu).

S.-Y. Park and P. R. Berger are with the Department of Electrical and Computer Engineering, The Ohio State University, Columbus, OH 43210, USA.

Digital Object Identifier 10.1109/TNANO.2007.908488

serve as a directly assembled nanocontact. Then, a Ni segment (100 to 300 nm) was electroplated using 0.5M nickel (II) sulfate (Alfa Aesar, Ward Hill, MA) solution with a Ni foil as the anode. Finally, a second Au nanowire segment ($\sim 3\ \mu$m) was electroplated using the same conditions, above the Ni segment to provide the second nanocontact. The Ag thin film and the Ag nanowire segment were then dissolved in 2M HNO_3. The sacrificial AAO template was finally dissolved in 1M NaOH, and the released nanowires were then concentrated using a centrifuge, and rinsed several times. The released all-metal nanowires were dispersed on an oxidized-Si substrates (SiO_2 thickness 1 μm; University Wafer, Boston, MA) and subsequently heat-treated at 600 °C for 0.5 h in air, to oxidize the Ni segment and fully convert it to NiO, while the two Au nanowire segments appear to be unaffected by this heat treatment.

B. Characterization

The Au–NiO–Au nanowires on the oxidized-Si substrates were observed in a scanning electron microscope (SEM) (Sirion, FEI, Hillsboro, OR) equipped with field emission source, operated at 15–20 kV accelerating voltage.

Specimens for transmission electron microscopy (TEM) examination were prepared by dispersing the Au–NiO–Au nanowires on TEM grids (Cu or Ni) covered with holey carbon (Quantifoil, Jena, Germany). The nanowires were observed in a conventional TEM (CM-200, Philips, Eindhoven, The Netherlands) equipped with an atmospheric thin-window energy dispersive spectrometer (EDS) (Phoenix System, EDAX, Mahwah, NJ), and a high-resolution TEM (HREM) (Tecnai F20, FEI, Hillsboro, OR) equipped with an postcolumn energy filter (Gatan, Pleasanton, CA), both operated at 200 kV accelerating voltage.

Simulated high-resolution images were created using commercially available EMS software package (Version 2.0105W2005, CIME-EPFL, Lausanne, Switzerland) [37]. The essential parameters used were: acceleration voltage 200 kV, spherical aberration coefficient $C_s = 1.3$ mm, chromatic aberration coefficient $C_c = 1.3$ mm, energy spread $\Delta E = 0.6$ eV, thickness $t = 2.0$ to 6.2 nm, and defocus $\Delta f = -45$ to -200 nm. Additionally, fast Fourier transform (FFT) patterns from the high-resolution TEM images, and corresponding simulated electron diffraction patterns, were obtained using commercially available software (Digital Micrograph, Gatan, Pleasanton, CA).

C. Device Fabrication and Electrical Properties Measurements

Au–NiO–Au nanowires dispersed on the oxidized-Si substrate were observed in the SEM-mode of the focused ion beam (FIB) (Strata 235 M Dual Beam, FEI, Hillsboro, OR), and high-quality single MOM nanowires were selected for device fabrication. Macroscopic contact pads of Pt were added atop each Au end of candidate Au–NiO–Au nanowires using the FIB's direct-write method described elsewhere [5], [13], [38]. Well-defined Pt contact lines (0.5 μm wide, 100 μm long) on both sides of the MOM nanowires were deposited at low Ga-ion beam current (100 pA) to minimize extraneous Pt "spatter." The beam current was then increased to 3–5 nA to deposit large contact pads ($20\ \mu\text{m} \times 50\ \mu\text{m}$) at the ends of the lines. A reference "shorted" device, without the nanowire, was also fabricated, where a 100 μm Pt line (0.5 μm wide) was deposited between two contact pads ($20\ \mu\text{m} \times 50\ \mu\text{m}$) on the oxidized-Si substrate.

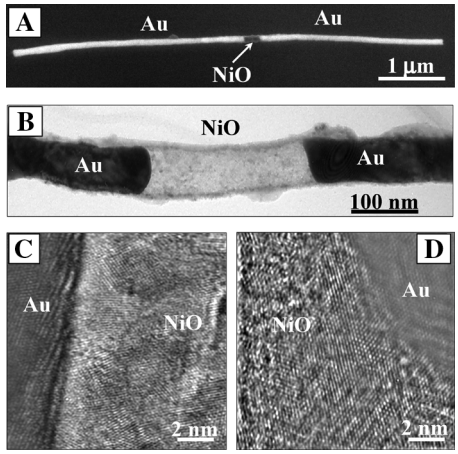

Fig. 1. (A) SEM micrograph of Au–NiO–Au nanowires synthesized in AAO templates with nanohole diameter of ~70 nm. (B) Bright-field TEM image of a Au–NiO–Au nanowire. High resolution TEM image of the (C) Au–NiO (left) and (D) NiO-Au (right) interfaces of the Au–NiO–Au nanowire in (B).

I–V responses of the single MOM nanowire devices were measured using a probe station (Alessi REL-4830HT, Cascade Microtech, Beaverton, Oregon) in conjunction with a parameter analyzer (HP 4156C with 410 expander chassis, Agilent Technologies, Santa Clara, CA). Tungsten probes with 1 μm tips were used to make intimate contact with the Pt pads. I–V characteristsics were measured by sweeping V from -4 V to $+4$ V in 40 mV steps, while measuring the corresponding I. Each device was subjected to up to 10 sweeps, before the I–V data, shown here, was recorded. I–V measurements were performed in ambient air, at 298 K, 373 K, 473 K, or 573 K.

III. Results and Discussion

Fig. 1(A) is a SEM micrograph of an isolated Au–NiO–Au nanowire, which is ~70 nm in diameter and $\sim$ 6.5 μm long. Fig. 1(B) is a bright-field TEM image of another isolated 70-nm diameter Au–NiO–Au nanowire, where the NiO segment is ~240 nm long. The Au–NiO interfaces appear sharp in this TEM micrograph. This is further corroborated by the HREM images in Fig. (1C) (left interface) and 1D (right interface) showing abrupt Au–NiO interfaces. The NiO segment is nanocrystalline, with a grain size of ~8 nm. The selected area electron diffraction pattern (SAEDP) in Fig. 2 confirms the presence of the cubic phase NiO (rocksalt structure) in the oxide segment. This is further confirmed by HREM studies of the NiO segment: Fig. 3 shows a HREM image of a NiO nanocrystal, along with the simulated image (center inset). The top-right inset is an indexed FFT pattern from the HREM image using the zone axis $[\bar{1}10]$. Although the majority of the oxide is the NiO stoichiometry, small amounts of Ni_2O_3 inclusions were observed.

Fig. 4(A) is a bright-field TEM image of the Au–NiO–Au nanowire [from Fig. 1(B)], while Fig. 4(B), 4(C), and 4(D) are energy-filtered elemental maps of O, Au, and Ni, respectively, of that nanowire. A combination of Fig. 4(B) and 4(D) shows

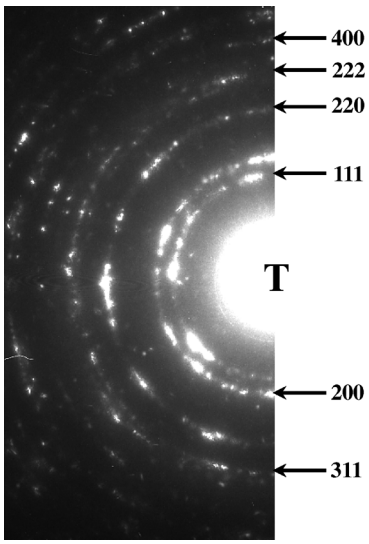

Fig. 2. SAEDP from the oxide segment indexed to cubic NiO. Transmitted spot denoted by T.

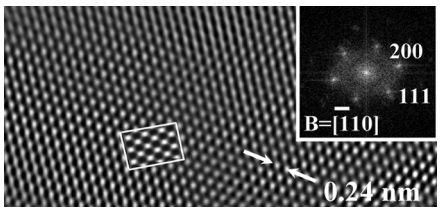

Fig. 3. High resolution TEM image of a NiO grain. Inset in the center is a simulated image. Inset on the right is FFT pattern (zone axis $[\bar{1}10]$) from the HREM image indexed to cubic NiO.

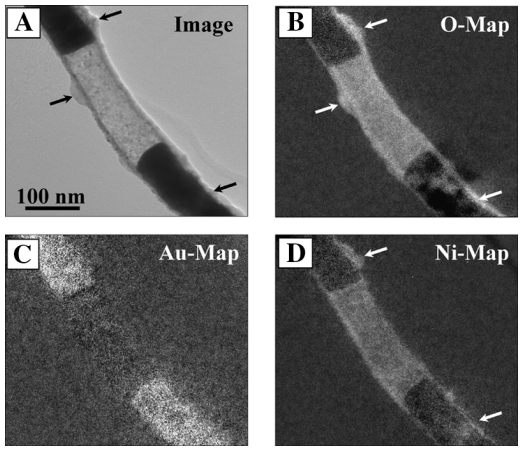

Fig. 4. (A) Bright-field TEM image of the Au–NiO–Au nanowire from Fig. 1(B). Corresponding elemental-map images of the Au–NiO–Au nanowire: (B) O, (C) Au, and (D) Ni. The top and bottom arrows in (A), (B), and (D) show the presence of a NiO surface sheath in the vicinity of the heterojunctions. The arrow in the center in (A) and (B) points to a surface oxide asperity that is not NiO.

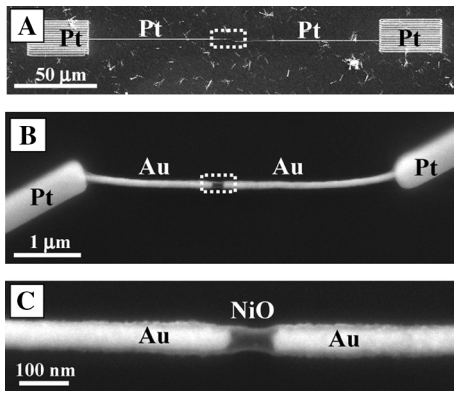

Fig. 5. (A) Low-magnification SEM image of the Au–NiO–Au nanowire device, showing the Pt contact pads and the Pt lines deposited using the FIB. (B) Higher magnification SEM image of the region within the dotted white rectangle in (A), showing the Pt lines making contact with the Au segments of the Au–NiO–Au nanowire. (C) High magnification SEM image of the region within the dotted white rectangle in (B), showing the Au–NiO–Au nanowire.

that there is a sheath of nickel oxide over the Au segment near the interface (top and bottom arrows). This could be due to surface diffusion of Ni during the heat-treatment followed by its oxidation. These figures also show that the asperity on the NiO segment (center arrow) is an oxide other than nickel oxide. It is possible that this asperity could be remnants of aluminum oxide from the AAO template. Fig. 4(C) shows clearly that there are no Au surface layers or Au nanograins on the NiO segment, precluding any obvious electrical shorting across the NiO segment. However, the presence of trace amounts of Au in the NiO segment below the detection limit of EDS ($<$1 at%) cannot be ruled out.

These characterization studies attest to the high quality of the Au–NiO–Au nanowires sythesized here. Furthermore, once optimized, the template-based method has the potential to produce large quantities of high-quality MOM nanowires of precise dimensions and architectures. The diameter of the nanowires can be adjusted by tuning the AAO nanohole diameters, which can, in principle, range from 20 to 400 nm. The total length of the MOM nanowires, and the lengths of the individual segments, can also be controlled precisely through careful sequential electroplating.

Fig. 5(A) is a low-magnification SEM image of the FIB-fabricated device, showing the Pt contact pads connected by Pt lines to a single Au –NiO–Au nanowire. Fig. 5(B) is a higher-magnification SEM image of the same region within the dashed-line rectangle in Fig. 5(A), showing the Pt-line contacts with the Au parts of the Au–NiO–Au nanowire. The long Au segments ensured that the NiO segment is far away from the Pt "spatter" (typically ~ 1 μm wide) that can be present around the Pt contacts lines. Fig. 5(C) is a high-magnification SEM image of the Au–NiO–Au nanowire, with a $\sim$70 nm diameter, $\sim$100 nm long NiO segment.

Fig. 6(A) shows room-temperature (298 K) I–V characteristics from the single Au–NiO–Au nanowire device pictured in Fig. 5, while Fig. 6(B) shows I–V responses from the same device at different temperatures. Fig. 6(C) shows room-temperature (298 K) I–V characteristics from a reference shorted device (not pictured here). Note that the ordinate scale (I) in Fig. 6(A) and 6(B) is in nA, while that in Fig. 6(C) is in mA. The ohmic I–V response of the reference shorted device in Fig. 6(C) and the five orders of magnitude higher current confirms the very low resistance $(\sim 4\ \text{k}\Omega)$ of the entire circuitry, including the FIB-deposited Pt-lines and the probe-tip contacts with the Pt pads. The I–V response from the bare substrate was found to be that of open circuit (not shown here). Thus, it can be concluded that the I–V responses in Fig. 6(A) and 6(B) are purely

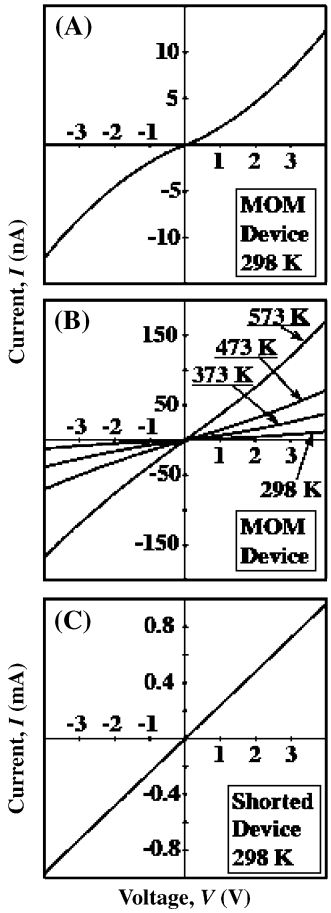

Fig. 6. I–V responses from the device pictured in Fig. 5 at: (A) 298 K and (B) at 298 K, 373 K, 473 K, and 573 K. (C) I–V response from the shorted device at 298 K. Note the vastly different ordinate (I) scales in the top [(A) and (B)] and the bottom (C) plots.

from the two back-to-back Au–NiO interfaces and the NiO segment itself.

In Fig. 6(A) the I–V response (at 298 K) is symmetric and somewhat nonlinear, with resistance of 62.5 MΩ at low voltage (±0.2 V), decreasing to 22.2 MΩ at high voltage (±3.8 V). The nonlinear, symmetric I–V curve indicates that the two back-to-back Au–NiO heterojunctions play an important role in determining the I–V response. Although the I–V response appears to be nonohmic, the MOM nanowires are not fully rectifying at low voltages. Full rectification is not expected with the Au–NiO heterojunctions because the Schottky barrier height (Φ_B) for the Au–NiO heterojuction is calculated to be quite small ∼0.34 eV $(\Phi_B = \chi_{\mathrm{NiO}} - \Phi_{\mathrm{Au}})$ [39], where the Au work function is $\Phi_{\mathrm{Au}} = 5.36$ eV [40] and the bottom of the NiO conduction band is $\chi_{\mathrm{NiO}} = 5.70$ eV [41]). Also, it should be noted that although the Au–NiO interface is sharp, and the Au segment of the nanowire is essentially single-crystal, the important NiO semiconductor segment is nanocrystalline and highly defective. These defects, whose electronic states are unknown, could provide hopping paths for carriers, resulting in the nonrectifying, yet nonlinear I–V, response observed in the Au–NiO–Au nanowire. It is expected that this effect would become more dominant with increasing temperature, which should lead to higher conductance and a more linear I–V response. This is exactly what is observed in Fig. 6(B).

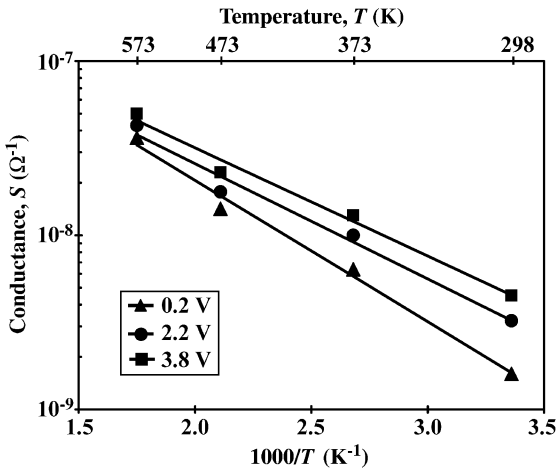

Fig. 7. Arrhenius type plot of conductance $(\sigma = I/V)$ versus $1000/T$ of the data in Fig. 6(B), for 0.2, 2.2, and 3.8 V applied voltages. The solid lines are linear fits to the data.

The data from Fig. 6(B) are replotted in Fig. 7 as conductance $(\sigma = I/V)$ versus $1/T$ in the Arrhenius form at low (0.2 V), medium (2.2 V), and high (3.8 V) applied voltages. At low voltage (0.2 V), the conductance increases about 23-fold with an increase in temperature from 298 to 573 K. That increase is about half (11-fold) at high applied voltage (3.8 V). Since the details of conduction mechanisms in these MOM nanowires are still unknown, the data in Fig. 7 is fitted to the simplest possible thermally activated conductance model, $\sigma = A\exp(-E_a/kT)$ [23], where A is the preexponential constant, E_a is the activation energy, and k is the Boltzmann constant. From the linear fits to the data in Fig. 7 the activation energies are found to be 0.16, 0.13, and 0.12 eV at applied voltages 0.2, 2.2, and 3.8 V, respectively. This decrease of E_a with increasing applied voltage is most likely because, at lower applied voltages, the overall conductance is expected to involve both, the two Au–NiO interfaces and the bulk NiO segment. While, at higher applied voltage, only the bulk NiO segment would be involved in conductance, resulting in a reduced activation energy.

IV. Summary

We have demonstrated the template-based synthesis of high-definition MOM heterojunction nanowires in the Au–NiO–Au system. Detailed electron-microscopy characterization studies of these nanowires show that the oxide segment is primarily cubic NiO and nanocrystalline, and that both the Au–NiO interfaces are well-defined. We were able to use a direct-write method for incorporating individual Au–NiO–Au nanowire easily in high-quality devices. The I–V response of individual Au–NiO–Au nanowires at room temperature was found to be nonlinear, but it became more linear and less resistive with increasing temperature.

Acknowledgment

Valuable experimental assistance from Dr. J.-J. Shyue, and Mr. E.D. Herderick is gratefully acknowledged.

References

[1] Z. W. Pan, Z. R. Dai, and Z. L. Wang, "Nanobelts of semiconducting oxides," *Science*, vol. 291, no. 5510, pp. 1947–1949, Mar. 9, 2001.

[2] Z. L. Wang, *Nanowires and Nanobelts—-Materials, Properties and Devices*. New York: Kluwer, 2003.
[3] Y. Xia, P. Yang, Y. Sun, Y. Wu, B. Mayers, B. Gates, Y. Yin, F. Kim, and H. Yan, "One-dimensional nanostructures: Synthesis, characterization, and applications," *Adv. Mater.*, vol. 15, pp. 353–389, 2003.
[4] A. Kolmakov and M. Moskovits, "Chemical sensing and catalysis by one-dimensional metal-oxide nanostructures," *Annu. Rev. Mater. Sci.*, vol. 34, pp. 151–180, 2004.
[5] J.-J. Shyue, R. E. Cochran, and N. P. Padture, "Transparent-conducting, gas-sensing nanostructures (nanowires, nanotubes, thin films) of titanium oxide synthesized at near-ambient conditions," *J. Mater. Res.*, vol. 21, pp. 2894–2903, 2006.
[6] R. E. Cochran, J. J. Shyue, and N. P. Padture, "Template-based, near-ambient synthesis of crystalline metal-oxide nanotubes, nanowires, and co-axial nanotubes," *Acta Mater.*, vol. 55, pp. 3007–3014, 2007.
[7] C. M. Lieber, "Nanoscale science and technology: Building big future from small things," *MRS Bull.*, vol. 28, pp. 486–491, 2003.
[8] W. S. Yun, J. J. Urban, Q. Gu, and H. Park, "Ferroelectric properties of individual barium titanate nanowires investigated by scanning probe microscopy," *Nano Lett.*, vol. 2, pp. 447–450, 2002.
[9] Z. L. Wang and J. Song, "Piezoelectric nanogenerators based on zinc oxide nanowire arrays," *Science*, vol. 312, pp. 242–246, 2006.
[10] C. Terrier, M. Abid, C. Arm, S. Serrano-Guisan, L. Gravier, and J.-P. Ansermet, "Fe_3O_4 nanowires synthesized by electroprecipitation in templates," *J. Appl. Phys.*, vol. 98, pp. 086102-1–086102-3, 2005.
[11] B. Lei, C. Li, D. Zhang, S. Han, and C. Zhou, "Efficient synthesis and electronic studies of core-shell nanowires based on collossal magneoresistance manganites," *J. Phys. Chem.*, vol. B 109, pp. 18799–18803, 2005.
[12] C. Li, D. Zhang, S. Han, X. Liu, T. Tang, B. Lei, Z. Liu, and C. Zhou, "Synthesis, electronic properties, and applications of indium oxide nanowires," *Mol. Elect. III Ann. New York Acad. Sci.*, vol. 1006, pp. 104–121, 2003.
[13] F. Hernandez-Ramirez, A. Tarancon, O. Casals, J. Rodriguez, A. Romano-Rodriguez, J. R. Morante, S. Barth, S. Mathur, T. Y. Choi, D. Poulikakos, V. Callegari, and P. M. Nellen, "Fabrication and electrical characterization of circuits based on individual tin oxide nanowires," *Nanotechnology*, vol. 17, pp. 5577–5583, 2006.
[14] C. Li, M. Curreli, H. Lin, B. Lei, F. N. Ishikawa, R. Datar, R. J. Cote, M. E. Thompson, and C. Zhou, "Complementary detection of prostate-specific antigen using in_2o_3 nanowires and carbon nanotubes," *J. Amer. Chem. Soc.*, vol. 127, pp. 12484–12485, 2005.
[15] J. S. Tresback, A. L. Vasiliev, and N. P. Padture, "Engineered metal–oxide–metal heterojunction nanowires," *J. Mater. Res.*, vol. 20, pp. 2613–2617, 2005.
[16] J.-J. Shyue and N. P. Padture, "Template-directed, near-ambient synthesis of Au–TiO_2–Au heterojunction nanowires mediated by self-assembled monolayers (sams)," *Mater. Lett.*, vol. 61, pp. 182–185, 2007.
[17] E. D. Herderick, J. S. Tresback, A. L. Vasiliev, and N. P. Padture, "Template-directed synthesis, characterization, and electrical properties of Au–TiO_2–Au heterojunction nanowires," *Nanotechnology*, vol. 18, pp. 155204-1–155204-6, 2007.
[18] N. I. Kovtyukhova, B. R. Martin, J. K. N. Mbindyo, P. A. Smith, B. Razavi, T. S. Mayer, and T. E. Mallouk, "Layer-by-layer assembly of rectifying junctions in and on metal nanowires," *J. Phys. Chem. B*, vol. 105, pp. 8762–8769, 2001.
[19] C. Kittel, *Introduction to Solid State Physics*. New York: Wiley, 1986.
[20] R. J. Powell and W. E. Spicer, "Optical properties of NiO and CoO," *Phys. Review B*, vol. 2, no. 6, pp. 2182–2193, Sep. 15, 1970.
[21] T. Satoh, N. P. Duong, and M. Fiebig, "Coherent control of antiferromagnetism in nio," *Phys. Rev. B*, vol. 74, p. 012404, 2006.
[22] L. Yuan, Z. P. Guo, K. Konstantinov, P. Munroe, and H. K. Liu, "Spherical clusters of nio nanoshafts for lithium-ion battery anodes," *Solid State Lett.*, vol. 9, pp. A524–A528, 2006.
[23] I. Hotovy, H. J. Huran, L. Spiess, R. Capkovic, and S. Hascik, "Preparation and characterization of nio thin films for gas sensor applications," *Vacuum*, vol. 58, pp. 300–307, 2000.
[24] J. A. Dirksen, K. Duval, and T. Ring, "NiO thin film formaldahyde gas sensor," *Sens. Actuators B*, vol. 80, pp. 106–115, 2001.
[25] I. Hotovy, V. Rehacek, P. Siciliano, S. Capone, and L. Spiess, "Characteristics of NiO thin films as NO_2 gas sensor," *Thin Solid Films*, vol. 418, pp. 9–15, 2002.
[26] W. Shin, M. Matsumiya, F. Qiu, N. Izu, and N. Murayama, "Thermoelectric gas sensor for detection of high hydrogen concentration," *Sens. Actuators B*, vol. 97, pp. 344–347, 2004.
[27] S. Noha, E. Lee, J. Seo, and M. Mehregany, "Electrical properties of nickel oxide thin films for flow sensor application," *Sens. Actuators*, vol. 125, pp. 363–366, 2006.
[28] G. Wakefield, P. J. Dobson, Y. Y. Foo, A. Loni, A. Simons, and J. L. Hutchinson, "Fabrication and characterization of nickel oxide films and their application as contacts to polymer/porous silicon electroluminescent devices," *Semicond. Sci. Technol.*, vol. 12, pp. 1304–1309, 1997.
[29] S. Berchmans, H. Gomathi, and G. P. Rao, "Electrooxidation of alcohols and sugars catalyzed on a nickel-oxide modified galss-carbon electrode," *J. Electroanal. Chem.*, vol. 394, pp. 267–270, 1995.
[30] C. R. Makkus, K. Hemmes, and J. H. W. Dewit, "A comparative study of NiO(Li), $LiFeO_2$, and $LiCoO_2$ porous cathodes for molten-carbonate fuel cells," *J. Electrochem. Soc.*, vol. 141, p. 3429, 1994.
[31] F. F. Ferreira, M. H. Tabacniks, M. C. A. Fantini, I. C. Faria, and A. Gorenstein, "Electrochromic nickel oxide thin films deposited under different sputtering conditions," *Solid State Ionics*, vol. 86–88, pp. 971–976, 1996.
[32] Y. Lin, T. Xie, B. Cheng, B. Geng, and L. Zhang, "Ordered nickel oxide nanowire arrays and their optical absorption properties," *Chem. Phys. Lett.*, vol. 380, pp. 521–525, 2003.
[33] Y. Zhan, C. Zheng, Y. Liu, and G. Wang, "Synthesis of nio nanowires by an oxidation route," *Mater. Lett.*, vol. 57, pp. 3265–3268, 2003.
[34] C. K. Xu, K. Q. Hong, S. Liu, G. H. Wang, and X. N. Zhao, "A novel wet chemical route to nio nanowires," *J. Cryst. Growth*, vol. 255, pp. 308–312, 2003.
[35] P. Yang, "The chemistry and physics of semiconductor nanowires," *MRS Bull.*, vol. 20, pp. 85–91, 2005.
[36] H. Cao, X. Qiu, Y. Liang, L. Zhang, M. Zhao, and Q. Zhu, "Sol-gel template synthesis and photoluminescence of n- and p-type semiconductor oxide nanowires," *Chem. Phys. Chem*, vol. 7, pp. 497–501, 2006.
[37] P. A. Stadelmann, "EMS—A software package for electron diffraction analysis and HREM image simulation in materials," *Ultramicroscopy*, vol. 21, pp. 131–146, 1987.
[38] V. Gopal, V. R. Radmilovic, C. Daraio, S. Jin, P. D. Yang, and E. A. Stach, "Rapid prototyping of site-specific nanocontacts by electron and ion beam assisted direct-write nanolithography," *Nano Lett.*, vol. 4, pp. 2059–2063, 2004.
[39] S. O. Kasap, *Principles of Electronic Materials and Devices*. New York: McGraw Hill, 2005.
[40] T. Okazawa, M. Fujiwara, T. Nishimura, T. Akita, M. Kohyama, and Y. Kido, "Growth mode and electronic structure of au nano-clusters on NiO (001) and TiO_2 (110)," *Surf. Sci.*, vol. 600, pp. 1331–1338, 2006.
[41] A. Erdemir, S. Li, and Y. Jin, "Relation of certain quantum chemical properties to lubrication behavior of solid oxides," *Int. J. Mol. Sci.*, vol. 6, pp. 203–218, 2000.

Jason S. Tresback received his B.S. degree in chemistry from the University of Massachusetts, Amherst, in 2002 and his M.S. degree in materials science and engineering from the University of Connecticut, Storrs, in 2005. He is currently working toward the Ph.D. degree in materials science and engineering at Ohio State University, Columbus.

His research interests are in nanoelectronics. He is currently fabricating and measuring electronic properties of devices that incorporate nanowire building blocks with functional oxides for a variety of applications.

Alexander L. Vasiliev received his Ph.D. degree in solid state physics and mathematics from the Institute of Crystallography, Russian Academy of Science, Moscow, in 1992.

He has held research positions at several institutes, including Russian Academy of Sciences; University of Antwerp, Belgium; Purdue University West Lafayette, IN; and University of Connecticut, Storrs, before joining Ohio State University, Columbus, in 2005 as a Postdoctoral Scholar. His research interests are in electron microscopy, crystallography, crystal defects, and interfaces.

Nitin P. Padture received the B.Tech. degree in metallurgical engineering from Indian Institute of Technology, Bombay, in 1985, his M.S. degree in ceramic engineering from Alfred University, Alfred, NY, in 1987, and his Ph.D. degree in materials science and engineering from Lehigh University, Bethlehem, PA, in 1991.

He was a Postdoctoral Scholar at the National Institute of Standards and Technology, before joining the University of Connecticut faculty in 1995. There he became a full Professor and Interim Department Head in 2003. He moved to Ohio State University, Columbus, as Professor of Materials Science and Engineering in January 2005. He has authored about 100 journal publications, including two papers in *Science* and 1 paper in *Nature Materials*, and he holds 3 patents. His papers average about 25 citations/publication, and six of his papers have received 100+ citations each. He has presented about 100 invited talks in the U.S. and abroad. His research interests include: i) structural ceramics, composites, and coatings, and ii) 1-D and 2-D functional nanomaterials and nanoelectronic devices.

Prof. Padture is a Fellow (2005) of the American Ceramic Society, and he has received that Society's Roland B. Snow (1990), Robert L. Coble (1998), and Richard M. Fulrath (2007) awards. He also received the Young Investigator award (1996) from the Office of Naval Research. He is a Principal Editor of the *Journal of Materials Research* and an Associate Editor of the *Journal of the American Ceramic Society*.

Si-Young Park (S'07) received the B.S. degree and the M.S. degree in Electrical and Computer Engineering from Ohio State University, Columbus, in 2003 and 2006, respectively. He is currently working toward the Ph.D. degree in Electrical and Computer Engineering at Ohio State University.

His research interests include plasma processing of Si-based nanoelectronics. His current research centers on Si/SiGe electronics for mixed-signal, mm-wave sensing, MODFET, and quantum dot nanoswitches.

Paul R. Berger (S'84-M'91-SM'97) received the B.S.E. degree in engineering physics in 1985, and the M.S.E. and Ph.D. degrees in electrical engineering in 1987 and 1990, respectively, all from the University of Michigan, Ann Arbor.

He is currently a Professor in both the Electrical and Computer Engineering Department and the Physics Department at the Ohio State University (2000-present). He is the Founder and Director of Ohio's new Nanoscale Patterning Laboratory and Co-Director of the Nanofabrication and Materials Processing Center (NanoMPC). Formerly, he worked at Bell Laboratories, Murray Hill, NJ (1990–'92) and taught at the University of Delaware in Electrical and Computer Engineering (1992–2000). In 1999, a sabbatical leave lead him to work at the Max-Planck Institute for Polymer Research, Mainz, Germany and Cambridge Display Technology, Ltd., Cambridge, United Kingdom. Currently, Dr. Berger is actively working on Si/SiGe nanoelectronic devices and fabrication processes; Si-based resonant interband tunneling diodes and quantum functional circuitry; conjugated polymer-based optoelectronic and electronic devices; molecular electronics; and semiconductor materials, fabrication, and growth. He has coauthored 80 archival refereed journal articles, 80 invited and regular conference presentations, three book sections and been issued ten patents with six more pending.

Dr. Berger has received an NSF CAREER Award (1996), a DARPA ULTRA Sustained Excellence Award (1998), and a Lumley Research Award (2006). He has been on the Program and Advisory Committees of numerous conferences, including the IEDM, ISDRS meetings. He currently is the Chair of the Columbus IEEE EDS/LEOS Chapter and Faculty Advisor to Ohio State's IEEE Student Chapter. He is also a member of the Optical Society of America and American Society for Engineering Education.